

# Bulk and surface critical behavior of a quantum Heisenberg antiferromagnet on two-dimensional coupled diagonal ladders

Zhe Wang,<sup>1</sup> Fan Zhang,<sup>1</sup> and Wenan Guo<sup>1,2,\*</sup>

<sup>1</sup>*Department of Physics, Beijing Normal University, Beijing 100875, China*

<sup>2</sup>*Beijing Computational Science Research Center, Beijing 100193, China*

 (Received 21 July 2022; revised 8 September 2022; accepted 29 September 2022; published 10 October 2022)

Using quantum Monte Carlo simulations, we study the spin-1/2 Heisenberg model on a two-dimensional lattice formed by coupling diagonal ladders. The model hosts an antiferromagnetic Néel phase, a rung singlet product phase, and a topological nontrivial Haldane phase, separated by two quantum phase transitions. We show that the two quantum critical points are all in the three-dimensional O(3) universality class. The properties of the two gapped phases, including the finite-size behavior of the string orders in the Haldane phase, are studied. We show that the surface formed by the ladder ends is gapless, while the surface exposed along the ladder is gapped in the Haldane phase. Conversely, in the gapped rung singlet phase, the former surface is gapped, and the latter is gapless. We demonstrate that, although the mechanisms of the two gapless modes are different, nonordinary surface critical behaviors are realized at both critical points on the gapless surfaces exposed by simply cutting bonds without fine-tuning the surface coupling required to reach a multicritical point in classical models. We also show that, on the gapped surfaces, the surface critical behaviors are in the ordinary class.

DOI: [10.1103/PhysRevB.106.134407](https://doi.org/10.1103/PhysRevB.106.134407)

## I. INTRODUCTION

At a bulk critical point, the surface may show rich and novel critical behaviors, called the surface critical behavior (SCB) [1]. The surface critical behavior is classified into three universality classes: ordinary, extraordinary, and special. Typically, the surface orders simultaneously with the bulk, and the surface singularities are purely induced by the bulk criticality. Therefore, the surface critical behavior is in the “ordinary” class. However, with enhanced surface couplings, the surface may be ordered by a surface transition while the bulk is disordered. At the bulk transition point, the ordered surface exhibits extra singularities; such a transition is in the “extraordinary” class. At a fine-tuned surface coupling strength, a multicritical point occurs between the two SCBs, known as the “special” class.

The subject of SCB has attracted numerous previous investigations [2,3] due to its rich and novel properties and recently obtained renewed attention when quantum phase transitions are involved. Zhang and Wang [4] studied the spin-1/2 Heisenberg model on a decorated square (DS) lattice and found a “nonordinary” SCB realized without fine-tuning the surface coupling. Based on the mapping between a  $d$ -dimensional quantum system and a  $(d + 1)$ -dimensional classical system, the surface of the two-dimensional (2D) SU(2) quantum model maps onto the 2D surface of the corresponding three-dimensional (3D) O(3) classical system, which cannot host a long-range order according to the Mermin-Wagner theorem [5]. As a result, there should be no SCB other than the ordinary one. Therefore, the nonordinary

SCB must have a purely quantum origin [4]. The authors attributed it to the property of the symmetry-protected topological (SPT) phase [6–8]; the gapless edge state of the SPT phase complemented with the critical mode of the bulk leads to a multicritical behavior.

Later studies on simple 2D dimerized spin-1/2 Heisenberg models found similar nonordinary SCBs on surfaces formed by dangling spins weakly coupled to the bulk, with surface critical exponents close to those of the nonordinary SCB found in the spin-1/2 DS Heisenberg model [9–11]. It was argued that the surface formed by dangling spins can be viewed as a spin-1/2 Heisenberg chain, which is gapless due to the topological  $\theta$  term of the spin-1/2 chain even if the bulk is in a trivial product state [9]. Such a gapless edge mode, together with the gapless bulk critical mode, leads to nonordinary SCBs. However, this scenario was challenged by the finding that the dangling surface of the  $S = 1$  dimerized Heisenberg model shows similar nonordinary exponents [12]. Naively, the surface is a spin-1 Haldane chain formed by dangling  $S = 1$  spins in this case, which is gapped.

In addition, the surface showing nonordinary SCBs of the spin-1/2 DS Heisenberg model is shown to be a dangling surface in a product state instead of an SPT state [10]. To check if the gapless edge state of an SPT phase can lead to similar nonordinary SCB, Zhu *et al.* [13] studied a 2D model of coupled spin-1 Haldane chains (CHC). In the path integral representation of the spin chain, the action has a topological term that is ineffective for integer spin- $S$  [14]. The chain is then described by the O(3) nonlinear sigma model without the topological term. However, this description only applies to the periodic boundary conditions. For an integer spin- $S$  chain with free boundaries, the action has a topological term of two spin-1/2 located at the ends of the chain [15]. For odd integer

\*waguo@bnu.edu.cn

S, the state is an SPT protected by certain symmetries [7]. When spin-1 chains are weakly coupled to form a 2D Haldane phase, which is the quasi-one-dimensional (1D) gapped phase that adiabatically connected to the Haldane phase in 1D as couplings between chains tend to 0. It was shown [16] that the phase is an SPT phase using the strange correlator method [17]. It is, therefore, natural to assume that the spin-1/2 excitations at the ends of the chains form a gapless edge state, according to the Lieb-Schultz-Mattis theorem [18]. This scenario was verified and used to explain the nonordinary SCB on the surface formed by the chain ends [13]. We emphasize that the surface is not formed by dangling spins. Instead, the gapless edge mode is due to a genuine SPT phase of the model. On the other hand, the SCB on the surface formed by a spin-1 chain is in the ordinary class.

Other mechanisms of such nonordinary SCB were also proposed [19–23]. In particular, an extraordinary-log SCB [19] is proposed and proved numerically [21] for a critical classical model in the 3D O(3) universality class. A special transition was found between the ordinary and extraordinary-log transitions, with exponents close to the nonordinary exponents of the quantum models. It was assumed that those quantum models are sitting close to the special transition point by chance and showing such special SCB at finite sizes [21].

In consideration of the current confusing research situation, to further investigate the origin of the nonordinary SCB in 2D quantum models, it would be beneficial to find/construct and study more 2D quantum SU(2) models with nonordinary SCBs existing at its 3D O(3) critical point. In this paper, we construct a model that hosts an SPT phase with nontrivial gapless surface states and a simple product phase with gapless mode on the surfaces formed by dangling spins. Notably, the two surfaces are different. Two quantum critical points in the 3D O(3) universality class separate the SPT phase and the product phase from the Néel phase in the middle. We show that the two gapless edge modes induce nonordinary SCBs *without fine-tuning surface couplings* on different surfaces with exponents agreed well at different bulk critical points.

The model is constructed by coupling the spin-1/2 diagonal ladders to form a 2D lattice, as illustrated in Fig. 1. A spin-1/2 diagonal ladder is shown in Fig. 1(a), which is the composite spin representation of a spin-1 chain, in the sense that the low-energy spectra of the two systems are identical [24]. The ground state of the diagonal ladder is gapped and unique if periodic boundary conditions are applied; however, it is fourfold degenerate for open boundary conditions due to spin-1/2 degrees of freedom living on the ends of the ladder. Experimentally, materials described by quasi-one-dimensional spin-1 chains or spin ladders have been found [25–27]. In the weak coupling region  $J_{\perp} \ll J$ , the model should stay in the Haldane phase. Similar to the coupled spin-1 chains [16], we expect the phase is an SPT phase with gapless edge modes. Indeed, at the surface formed [Y surfaces shown in Fig. 1(b)] by the ends of the ladders, we observe gapless surface states (see Sec. III B). When the coupling  $J_{\perp}$  is strong enough, the model goes to the trivial product state: rung singlet phase (RS), which has a gapless mode on the surface formed by dangling spins [X surfaces, see Fig. 1(c)]. Since the lattice is bipartite, when the couplings between the ladders are

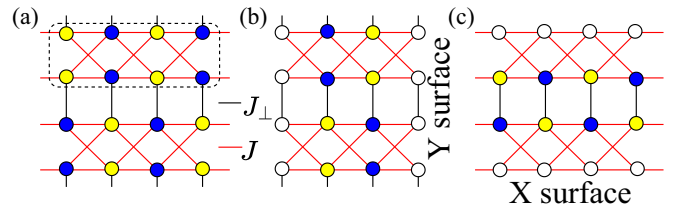


FIG. 1. Two-dimensional coupled diagonal ladders. A diagonal ladder is shown inside the dashed rectangular box. The lattice is bipartite with sublattices A (yellow circles) and B (blue circles). (a) Periodic boundary conditions are applied in the  $x$  and  $y$  directions. (b) Periodic boundary conditions are applied in the  $y$  direction, while open boundaries are applied in the  $x$  direction to expose the Y surfaces. (c) Periodic boundary conditions are used in the  $x$  direction, while open boundary conditions are applied in the  $y$  direction to expose the X surfaces. Open circles denote spins on the surfaces. The intraladder couplings  $J > 0$  are indicated by red lines, and interladder couplings  $J_{\perp} > 0$  by black lines.

competitive with the couplings inside the ladders, the model should stay in the Néel phase. The three phases are separated by two quantum critical points (QCPs). The phase diagram is sketched in Fig. 2.

Using unbiased quantum Monte Carlo (QMC) simulations [28,29], we determine the two quantum critical points and show that they belong to the 3D O(3) universality class regardless of whether the nonmagnetic phase is an SPT phase or a trivial product phase. We demonstrate that nonordinary SCBs are realized at the two bulk critical points but on different surfaces, which are exposed by simply cutting bonds without fine-tuning the surface couplings required to reach a multicritical point in the classical models. We study the properties of the two gapped phases, including the finite-size behavior of the string orders in the Haldane phase. We show that the surface formed by the ladder ends is gapless in the Haldane phase, on which the nonordinary SCB is observed; the surface along the chain direction is gapped; therefore, the SCB on it is ordinary. However, in the RS phase, the latter surface becomes a chain formed by dangling spins and gapless. Therefore, we found nonordinary SCB on it instead.

The paper is organized as follows. In Sec. II, we describe our model and the methods used in our study. Section III presents a phase of the diagram and bulk quantum phase

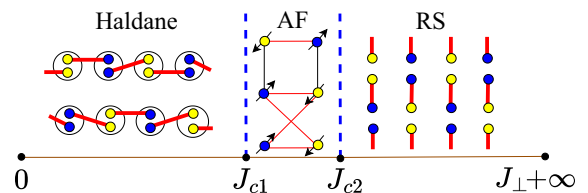


FIG. 2. Phase diagram with three phases: the antiferromagnetic phase (AF), the Haldane phase, and the rung singlet phase (RS), separated by two quantum critical points  $J_{c1}$  and  $J_{c2}$ . A cartoon of a representative ground state is graphed in each phase. The arrows represent the orientation of spins. Thick-red lines denote spin singlets. The circles in the Haldane phase indicate that two spins-1/2 form a spin-1.

transitions of the model. Topological properties of the Haldane phase and surface properties of the surfaces in two magnetic disordered phases are also studied. In Sec. IV, we study the surface critical behaviors of our model. Finally, we present our conclusions and discuss the mechanisms of the origins of nonordinary surface critical behavior in Sec. V.

## II. MODELS AND METHODS

We study the spin-1/2 Heisenberg model on a designed two dimensional bipartite lattice constructed by coupling diagonal ladders [24]; see Fig. 1(a). We will refer to the lattice as coupled diagonal ladders (CDLs). The Hamiltonian is given by

$$H = \sum_{j=0} H_j + J_{\perp} \sum_{i,j=0} \mathbf{S}_{i,2j+1} \cdot \mathbf{S}_{i,2(j+1)}, \quad (1)$$

where the first sum is over the diagonal ladders with  $H_j$  describing the  $j$ th ladder written as follows:

$$H_j = J \sum_{l=0,1} \sum_i \mathbf{S}_{i,2j+l} \cdot \mathbf{S}_{i+1,2j+l} + J \sum_i [\mathbf{S}_{i,2j} \cdot \mathbf{S}_{i+1,2j+1} + \mathbf{S}_{i,2j+1} \cdot \mathbf{S}_{i+1,2j}], \quad (2)$$

where  $l = 0, 1$  denote two legs of the  $j$ th diagonal ladder and  $J > 0$  is intraladder Heisenberg exchange interactions. The second sum describes the coupling of the neighboring ladders with the interladder couplings  $J_{\perp} > 0$ .

We set  $J$  to be unity. When  $J_{\perp}$  is comparable to  $J$ , the model is expected in the Néel phase. For the limit  $J_{\perp} \gg 1$ , the model is tuned into a disordered rung singlet phase (RS), a product of singlets. On the other limit,  $J_{\perp} \rightarrow 0$ , the model is tuned into a gapped Haldane phase, which can be described by the AKLT state. These three phases are separated by two quantum critical points, as sketched in Fig. 2.

The lattice is bipartite; therefore, the model is free of magnetic frustration and can be studied using quantum Monte Carlo simulations. In this paper, we use stochastic series expansion (SSE) quantum Monte Carlo simulations with the loop algorithm [28,29] to study the bulk and surface properties of the gapped phases, as well as the bulk and surface critical behaviors. Periodic boundary conditions are applied along both the  $x$  and  $y$  directions when the bulk phase transitions are studied. When the surface states and surface critical behaviors are studied, periodic boundary conditions are applied along one lattice direction and open boundary conditions are used along the other direction to expose the surfaces, as shown in Figs. 1(b) and 1(c). The Y surfaces are obtained by cutting the lattice along the  $y$  direction. Similarly, we can expose the X surfaces by cutting the lattice along the  $x$  direction. Note that for the X surfaces, we only consider the case of cutting  $J_{\perp}$  bonds.

In our simulations, we have reached linear size up to  $L = 128$ . The inverse temperature scales as  $\beta = 2L$ , considering the dynamic critical exponent  $z = 1$  for the two critical points. Typically  $10^8$  Monte Carlo samples are taken for each coupling strength.

## III. BULK RESULTS

### A. Bulk phases and properties of associated bulk critical points

We study several physical quantities to investigate the bulk phases and related phase transitions. The two transitions are associated with the spontaneous breaking of the spin rotational symmetry. The staggered magnetization is used to describe the Néel order,

$$m_s^z = \frac{1}{L^2} \sum_i \phi_i S_i^z, \quad (3)$$

where the staggered phase factor  $\phi_i = \pm 1$  according to the sublattice to which site  $i$  belongs. The Binder cumulant  $U_2$  [30,31] is defined using  $m_s^z$ ,

$$U_2 = \frac{5}{6} \left( 3 - \frac{\langle (m_s^z)^4 \rangle}{\langle (m_s^z)^2 \rangle^2} \right), \quad (4)$$

which is dimensionless at the critical point.  $U_2$  converging to 1 with increasing system size indicates the existence of magnetic order, while tending to zero with increasing system size implies that the system is in the magnetic disordered phase.

The mean spin stiffness  $\rho_s$  over the  $x$  and  $y$  directions is also calculated. It is related to the fluctuations of the winding number [32,33],

$$\rho_s = \frac{3}{4} \langle W_x^2 + W_y^2 \rangle / \beta, \quad (5)$$

where

$$W_a = \frac{1}{L_a} (N_a^+ - N_a^-) = 0, \pm 1, \pm 2, \dots \quad (6)$$

is the winding number along the  $a = x, y$  direction. Here,  $N_a^+$  and  $N_a^-$  denotes the total number of operators transporting spin in the positive and negative  $a$  direction, respectively.

$\rho_s$  is nonzero if the state is magnetically ordered and goes to zero when the system is in the magnetically disordered phase. The size dependence of the spin stiffness exactly at a QCP is expected as follows [34]:

$$\rho_s \sim L^{2-(d+z)}, \quad (7)$$

where  $z$  is the dynamic exponent and  $d = 2$  are the dimensions of the model. In the case that  $z = 1$ ,  $\rho_s L$  is expected to be dimensionless at the critical point.

Figure 3 plots  $\rho_s L$  and  $U_2$  as functions of  $J_{\perp}$  for different system sizes. Clearly, the model is in the antiferromagnetic ordered state when  $J_{\perp}$  is between 0.17 and 3. Since  $U_2$  and  $\rho_s L$  are dimensionless at a critical point, the crossings of curves for different sizes roughly indicate two transition points.

We adopt the standard  $(L, 2L)$  crossing analysis for  $U_2$  and  $\rho_s L$  to estimate the critical point and critical properties, see, e.g., the Supplemental Material of [35]. For  $Q = U_2$  or  $\rho_s L$ , we define the finite-size estimator of the critical points  $J_c^{(Q)}(L)$  as the crossing point of the  $Q(J_{\perp})$  curves for  $L$  and  $2L$ , which drifts toward the critical point  $J_c$  in the thermodynamic limit in the following way:

$$J_c^{(Q)}(L) = J_c + aL^{-1/\nu-\omega}, \quad (8)$$

where  $\nu$  is the correlation length exponent,  $\omega > 0$  is the effective irrelevant exponent, and  $a$  is an unknown constant. At the

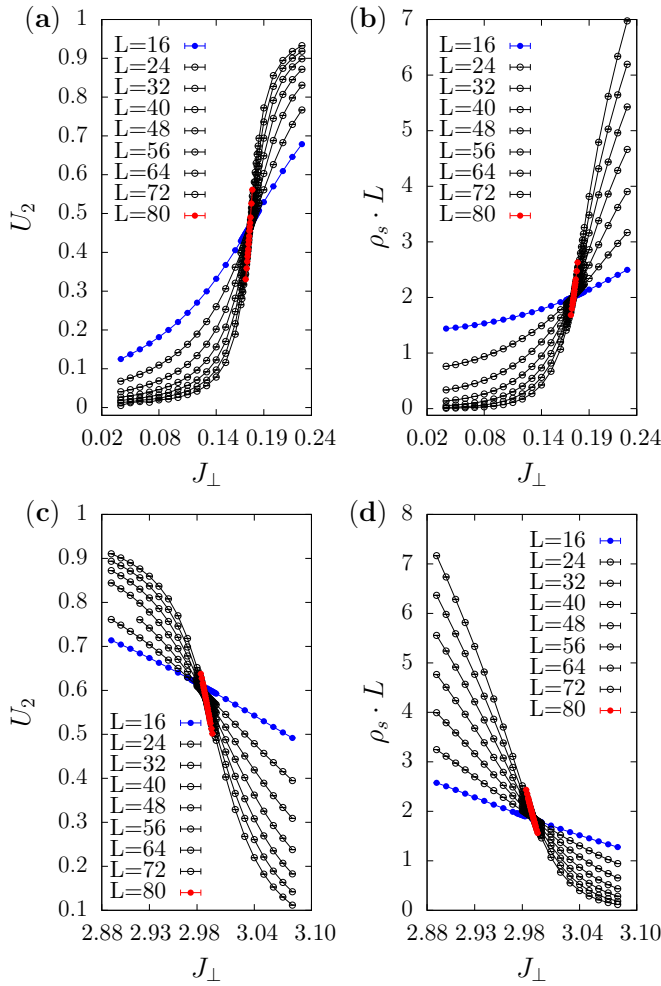


FIG. 3. Binder cumulant  $U_2$  and spin stiffness multiplied by the system size  $\rho_s L$  vs  $J_\perp$  for different system sizes. Error bars are much smaller than the symbols. [(a),(b)] Show the results near the critical point  $J_{c1}$ . [(c),(d)] Show the results near critical point  $J_{c2}$ .

crossing point  $J_c^{(Q)}(L)$ , we define the finite-size estimator of exponent  $\nu$  as

$$\frac{1}{\nu^{(Q)}(L)} = \frac{1}{\ln 2} \ln \left( \frac{s^{(Q)}(2L)}{s^{(Q)}(L)} \right) \quad (9)$$

where  $s^{(Q)}(L)$  is the slope of the curve  $Q(J_\perp)$  for size  $L$  at  $J_c^{(Q)}(L)$ .  $\nu^{(Q)}(L)$  converges to the exponent  $\nu$  in the following

way:

$$\nu^{(Q)}(L) = \nu + bL^{-\omega}, \quad (10)$$

with  $b$  an unknown constant.

For  $U_2$  and  $\rho_s L$ , the analyses yield consistent estimates of  $J_c$  and  $\nu$  within error bars. The results with higher accuracy are selected as the final results. All the results are listed in Table I. In particular, the final estimates of the two critical points are  $J_{c1} = 0.17425(3)$  and  $J_{c2} = 2.99046(5)$ .

To further determine the universal properties of the two critical points, we calculate the static spin structure factor and the spin correlation at the longest distance in a finite system at the two estimated critical points  $J_{c1}$  and  $J_{c2}$ . The two quantities are defined based on the spin correlation function

$$C(\mathbf{r}_{ij}) = \langle S_i^z S_j^z \rangle, \quad (11)$$

where  $\mathbf{r}_{ij}$  is the vector from site  $i$  to  $j$ . The static spin structure factor at wave vector  $(\pi, \pi)$  is defined as follows:

$$S(\pi, \pi) = \sum_{\mathbf{r}} \epsilon_{ij} C(\mathbf{r}_{ij}), \quad (12)$$

where  $\epsilon_{ij} = \pm 1$ , depending on whether  $i$  and  $j$  belong to the same sublattice. The spin correlation function of the half lattice size  $C(L/2, L/2)$  averages  $C(\mathbf{r}_{ij})$  between two spins  $i$  and  $j$  at the longest distance  $\mathbf{r}_{ij} = (L/2, L/2)$ .

$S(\pi, \pi)$  and  $C(L/2, L/2)$  are used to extract the scaling dimension  $y_h$  of the staggered magnetic field  $h$  and the anomalous dimension  $\eta$ . At QCP,  $S(\pi, \pi)$  and  $C(L/2, L/2)$  satisfy the following finite size scaling forms:

$$S(\pi, \pi)/L^2 \sim L^{-2(d+z-y_h)}(1 + bL^{-\omega}), \quad (13)$$

and

$$C(L/2, L/2) \sim L^{-(d+z-2+\eta)}(1 + bL^{-\omega}), \quad (14)$$

respectively, in which  $d = 2$  is the spatial dimension,  $z = 1$  is the dynamical critical exponent, and  $\omega$  is the effective correction to scaling exponent. The two exponents  $y_h$  and  $\eta$  are not independent and are expected to obey the following scaling relation:

$$\eta = d + z + 2 - 2y_h. \quad (15)$$

TABLE I. Bulk critical properties. The exponents obtained by field theory (FT) and by Monte Carlo simulations (MC) are listed for comparison.

	$J_c$	$\nu$	$\eta$	$y_h$
$J_{c1}$	0.17425(3)	0.707(48)	0.033(6)	2.484(1)
$J_{c2}$	2.99046(7)	0.705(6)	0.0324(34)	2.483(1)
FT [36]		0.7073(35)	0.0355(25)	
MC [37]		0.7117(5)	0.0378(3)	

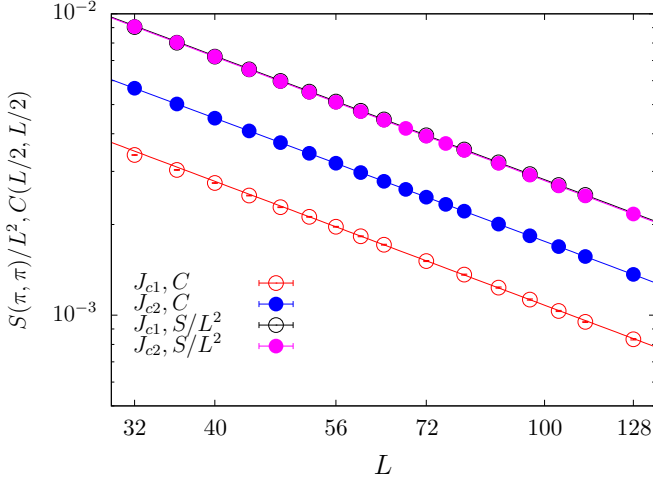


FIG. 4.  $C(L/2, L/2)$  and  $S(\pi, \pi)/L^2$  vs system size  $L$  at quantum critical points  $J_{c1}$  and  $J_{c2}$  on a log-log scale. The symbols of  $S/L^2$  at  $J_{c1}$  are covered by those at  $J_{c2}$ . Error bars are much smaller than the symbols.

The numerical results of  $S(\pi, \pi)/L^2$  and  $C(L/2, L/2)$  as functions of system size  $L$  at two critical points are shown in Fig. 4. We fit the data of  $S(\pi, \pi)/L^2$  and  $C(L/2, L/2)$  according to Eqs. (13) and (14), respectively, and find the critical exponents  $y_h$  and  $\eta$ , as listed in Table I. The obtained  $y_h$  and  $\eta$  satisfy the scaling relations Eq. (15).

Compared with the best-known exponents of the 3D  $O(3)$  universality class [36,37], we conclude that both critical points belong to the 3D  $O(3)$  universality class. This also shows that the topological order does not change the universality class of the bulk phase transition.

### B. Properties of the Haldane phase and its surface states

The spin-1/2 Heisenberg diagonal ladder is shown as the composite spin representation of a spin-1 chain [24] by representing the spin-1 operator  $\sigma_i$  of the chain as the sum of two spin-1/2 operators  $\sigma_i = \mathbf{S}_{i,0} + \mathbf{S}_{i,1}$  on two legs, as illustrated in Fig. 5. The low-energy spectrum of the ladder is identical to that of the spin-1 chain. When periodic boundary conditions are applied, all spins are bound to form valence bonds and the ground state is unique. The ground state of this ladder can be well described by the AKLT state [38], which is a short-ranged valence-bond (VB) state. A typical configuration is shown in Fig. 2. The Haldane gap is related to the energy needed to break a valence bond. More importantly, with open boundaries, the ground states have two spin-1/2 spins localized at the ends of the ladder. This is evident in the diagonal ladders as shown in Fig. 5. The ladder is in a Haldane phase with symmetry protected topological order.

The Haldane phase with symmetry protected topological order is characterized by a nonlocal string order, which is evident when the  $z$  component of the spins on the same rung are summed. The total  $S_i^z = S_{i,0}^z + S_{i,1}^z$  can take the values of 1, 0, -1. When the sites with  $S_i^z = 0$  are removed, the remaining sites have an Néel order, which means a string order, as shown in Fig. 5(a). This order can be described by the following

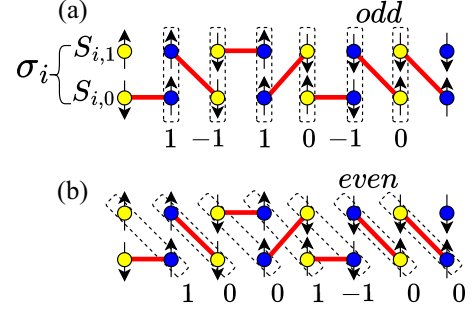


FIG. 5. A representation of VB ground state with two spin-1/2 localized at the ends of the ladder and a spin configuration matches the VB state. (a) Dashed boxes encircle rungs:  $S_i^z = S_{i,0}^z + S_{i,1}^z$ , used to calculate the string order parameter  $\mathcal{S}_{\text{odd}}$ . After all sites with  $S_i^z = 0$  is removed, the remaining sites show Néel order. (b) Dashed boxes encircle diagonals:  $S_i^z = S_{i+1,0}^z + S_{i,1}^z$ , used to calculate the string order parameter  $\mathcal{S}_{\text{even}}$ . After all sites with  $S_i^z = 0$  removed, the remaining sites do not show Néel order.

string order parameter [24,39]:

$$\mathcal{S}_{\text{odd}}(i, j) = \left\langle (S_{i,0}^z + S_{i,1}^z) \times \exp \left( i\pi \sum_{k=i+1}^{j-1} (S_{k,0}^z + S_{k,1}^z) \right) (S_{j,0}^z + S_{j,1}^z) \right\rangle. \quad (16)$$

The name  $\mathcal{S}_{\text{odd}}$  comes from the topology of the VBs in the diagonal ladder [24], which is determined by the parity of the number of VBs crossing an arbitrary vertical line. Note that the VB state shown in Fig. 5 is odd.

Other ladders in the Haldane phase may show a topologically distinct string order, which can be defined as

$$\mathcal{S}_{\text{even}}(i, j) = \left\langle (S_{i+1,0}^z + S_{i,1}^z) \times \exp \left( i\pi \sum_{k=i+1}^{j-1} (S_{k+1,0}^z + S_{k,1}^z) \right) \times (S_{j+1,0}^z + S_{j,1}^z) \right\rangle, \quad (17)$$

which is nonzero when the VB configuration is even, i.e., an even number of VBs crossing an arbitrary vertical line [24]. In the case of the diagonal ladder, as shown in Fig. 5(b), when the  $z$  component of the spins along the plaquette diagonals are summed, there is no such a string order. Apparently, the parity of the VB ground state is intimately related to the type of string order.

The finite value of a string order parameter at the limit  $|i - j| \rightarrow \infty$  characterizes a stable topological order in the thermodynamic limit. In the simulations of a system of size  $L$  with periodic boundaries, we calculate  $\mathcal{S}_{\text{odd}}(L/2)$  [ $\mathcal{S}_{\text{even}}(L/2)$ ] by averaging  $\mathcal{S}_{\text{odd}}(i, j)$  [ $\mathcal{S}_{\text{even}}(i, j)$ ] at the maximum available distance  $|i - j| = L/2$  along an individual ladder. As shown

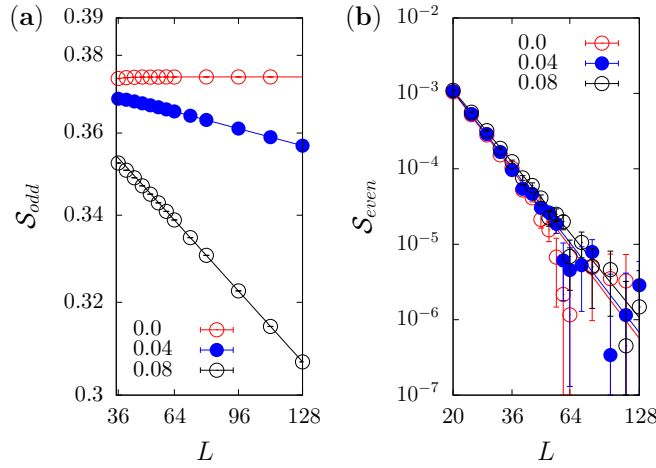


FIG. 6. String order parameters  $S_{\text{odd}}(L/2)$  (a) and  $S_{\text{even}}(L/2)$  (b) of the 2D coupled diagonal ladders at different interladder couplings  $J_{\perp}$  in the SPT Haldane phase. (a) On a linear-log scale. (b) On a log-log scale.

in Figs. 6(a) and 6(b), in the case  $J_{\perp} = 0$ ,  $S_{\text{odd}}(L/2)$  is finite,  $S_{\text{even}}(L/2)$  vanishes when  $L$  goes infinity, as expected for a diagonal ladder. We find that  $S_{\text{odd}}$  converges to 0.374325(7).

Now consider that the diagonal ladders are coupled to form a 2D lattice by interladder couplings  $J_{\perp} > 0$ . Due to the Haldane gap, the properties of the ground state are robust against a weak higher-dimensional coupling between ladders. There is no phase transition when  $J_{\perp}$  is turned on to finite values less than  $J_{c1}$ . This means that the model has a gapped Haldane phase that is adiabatically connected to the AKLT states of diagonal ladders. However, it was theoretically predicted that the string order of the coupled spin-1 Haldane chains is not stable and decays exponentially for arbitrarily weak interchain coupling [40]. This prediction has been verified numerically recently in the 2D CHC model [13] for sufficiently large system sizes.

We obtain similar results in the SPT Haldane phase of the current model. We find that the string order parameter  $S_{\text{odd}}(L/2)$  decays exponentially with  $L$ , but much slower than the decay of the string order parameter in the CHC model at the same interladder/interchain couplings. The numerical results are shown in Fig. 6(a). Fitting according to the following formula [40]:

$$S_{\text{odd}}(L/2) \sim \exp(-\alpha L/2), \quad (18)$$

we find  $\alpha = 0.0007437(8)$  for  $J_{\perp} = 0.04$ , and  $\alpha = 0.003089(1)$  for  $J_{\perp} = 0.08$ .

We also calculated  $S_{\text{even}}(L/2)$  inside the Haldane phase. As expected, the even string order parameter values are much smaller than the odd values. However, interestingly, we find that  $S_{\text{even}}(L/2)$  decays algebraically with system size, as shown in Fig. 6(b). We have tried to fit the data using the following scaling form:

$$S_{\text{even}}(L/2) \sim L^{-\beta}, \quad (19)$$

and find  $\beta = 4.2(1)$  for a single ladder,  $\beta = 3.97(5)$  at  $J_{\perp} = 0.04$ , and  $\beta = 3.74(3)$  at  $J_{\perp} = 0.08$ .

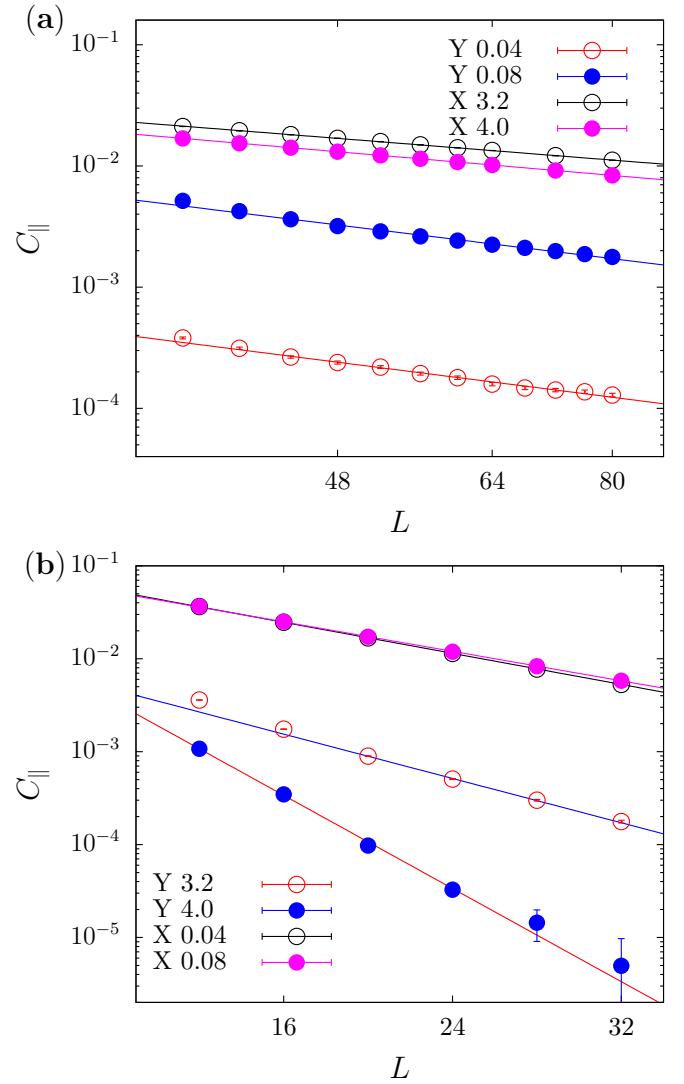


FIG. 7. Surface correlation  $C_{\parallel}(L/2)$  vs system size  $L$ . (a) Y surface in the Haldane phase ( $J_{\perp} = 0.04, 0.08$ ) and X surface in the RS phase ( $J_{\perp} = 3.2, 4.0$ ). The plot is on a log-log scale. Algebraically decaying with  $L$  is seen, showing gapless surface states. (b) Y surface in the RS phase and X surface in the Haldane phase. The plot is set on a linear-log scale. Exponential decaying with  $L$  is observed, meaning that the surface states are gapped.

However, the hallmark of the SPT phase is not the string order, but the presence of nontrivial surface states that are gapless or degenerate. Our model is spatially anisotropy, and we consider two different surfaces, the Y surface and the X surface, exposed by cutting the lattice; see Fig. 1. To study the surface states, we calculate the surface parallel correlation  $C_{\parallel}(L/2)$ , which averages  $C(\mathbf{r}_i; j)$  between the two surface spins  $i$  and  $j$  at the longest distance  $L/2$ .

The results for the Y surface at two couplings  $J_{\perp}$  in the SPT phase are plotted in Fig. 7(a). We see that  $C_{\parallel}(L/2)$  decays with system size  $L$  in a power law,

$$C_{\parallel}(L/2) \sim L^{-p} \quad (20)$$

with  $p = 1.30(4)$  at  $J_{\perp} = 0.04$  and  $p = 1.12(2)$  at  $J_{\perp} = 0.08$ , meaning that the surface states are gapless. Although the Y

surface is strongly coupled to the bulk at this phase, it is easy to understand from the AKLT state shown in Fig. 5(a). With open boundaries, each ladder carries a spin-1/2 excitation at each end. A gapless surface state described by a (1+1)-dimensional gapless critical theory is formed at the Y surface by coupling these spin-1/2 excitations, according to the Lieb-Schultz-Mattis theorem [18].

Meanwhile, the results of  $C_{\parallel}(L/2)$  for the X surface at the same two couplings in the SPT phase have completely different finite-size behavior, as shown in Fig. 7(b). The data can be fitted using straight lines on a linear-log scale, meaning the correlation decays exponentially. Fitting the curves with

$$C_{\parallel}(L/2) \sim \exp(-L/a), \quad (21)$$

we obtain  $a = 10.56(2)$  at  $J_{\perp} = 0.04$  and  $a = 11.49(3)$  at  $J_{\perp} = 0.08$ . The surface states on the X surface are gapped, because the X surface is a gapped diagonal ladder, in its AKLT state, weakly coupled to the bulk.

### C. Surface states of the trivial rung singlet product phase

Now we move to the RS phase with  $J_{\perp} > J_{c2}$ . The nature of this trivial disordered phase can be understood by examining the limit  $J_{\perp} \rightarrow \infty$ , at which the lattice reduces to disjoint bonds, see Fig. 2. The ground state is the direct product of these rung singlets.

We have calculated  $C_{\parallel}(L/2)$  along the Y surface. The results are plotted in Fig. 7(b). We see the correlations at  $J_{\perp} = 3.2$  and  $J_{\perp} = 4.0$  decaying exponentially. Fitting data according to Eq. (21), we find  $a = 7.2(2)$  and  $3.46(6)$ , respectively, indicating that the Y surface states are gapped. Apparently, the surface can be understood as sitting in a state adiabatically connected to a product state of dimers.

However, the X surface can be considered a chain of dangling spins, weakly coupled to the bulk, in the RS phase. Thus, we expect the surface states to be gapless, forming a spin-1/2 Heisenberg chain. This is proven by our numerical results. As shown in Fig. 7(a), the correlation  $C_{\parallel}(L/2)$  along the X surface at  $J_{\perp} = 3.2$  and  $4.0$  decay in a power law. Fitting according to Eq. (20), we obtain the powers  $p = 0.827(2)$  and  $0.886(2)$ , respectively.

## IV. SURFACE CRITICAL BEHAVIORS

We now study the surface critical behaviors on the X and Y surfaces at the two bulk critical points. In addition to the surface correlation  $C_{\parallel}(L/2)$ , we also calculate another spin-spin correlation  $C_{\perp}(L/2)$  and the surface staggered magnetic susceptibility  $\chi_{s1}$  with respect to the surface field  $h_1$ .

$C_{\perp}(L/2)$  averages  $C(\mathbf{r}_{ij})$  between spin  $i$  fixed on the surface and spin  $j$  located at the center of the bulk, with  $\mathbf{r}_{ij}$  perpendicular to the surface with  $|j - i| = L/2$ .

$\chi_{s1}$  can be calculated through the Kubo formula [28]

$$\chi_{s1} = \frac{\partial \langle m_{s1}^z \rangle}{\partial h_1} = L \int_0^\beta d\tau \langle m_{s1}^z(\tau) m_{s1}^z(0) \rangle, \quad (22)$$

TABLE II. Surface critical exponents at different surface configurations.

Configuration	$y_{h1}$	$\eta_{\parallel}$	$\eta_{\perp}$
Y-c1	1.756(3)	-0.511(2)	-0.237(2)
Y-c2	0.852(46)	1.318(31)	0.682(9)
X-c1	0.82(1)	1.36(6)	0.69(3)
X-c2	1.780(2)	-0.56(1)	-0.259(3)

where  $m_{s1}^z$  is the staggered surface magnetization defined as follows:

$$m_{s1}^z = \sum_{i \in \text{surface}} \phi_i S_i^z, \quad (23)$$

where the summation is restricted on the surface,  $\phi_i = \pm 1$  depending on the sublattice to which  $i$  belongs.

At bulk critical points, the finite-size scaling behavior of the two correlations is characterized by two anomalous dimensions  $\eta_{\parallel}$  and  $\eta_{\perp}$ ;

$$C_{\parallel}(L/2) \sim L^{-(d+z-2+\eta_{\parallel})} (1 + b_1 L^{-\omega}), \quad (24)$$

and

$$C_{\perp}(L/2) \sim L^{-(d+z-2+\eta_{\perp})} (1 + b_2 L^{-\omega}), \quad (25)$$

where  $\omega$  is the effective exponent of corrections to scaling and  $b_1$  and  $b_2$  are unknown constants. The susceptibility  $\chi_{s1}$  has the following scaling form:

$$\chi_{s1} \sim L^{-(d+z-1-2y_{h1})} (1 + b L^{-\omega}), \quad (26)$$

where  $y_{h1}$  is the scaling dimension of the surface field  $h_1$ ,  $\omega$  is the effective exponent of corrections to scaling, and  $b$  is an unknown constant. For our model,  $d = 2$  and  $z = 1$ .  $\omega = 1$  yields good fitting for all critical exponents.

The three exponents  $y_{h1}$ ,  $\eta_{\parallel}$ , and  $\eta_{\perp}$  are related through the following scaling relations [3]:

$$2\eta_{\perp} = \eta_{\parallel} + \eta \quad (27)$$

and

$$\eta_{\parallel} = d + z - 2y_{h1}, \quad (28)$$

where  $\eta$  is the anomalous magnetic scaling dimension of the bulk critical point in the  $d + z$  spacetime.

In the remainder of this section, we use these physical quantities to examine SCBs. Two ordinary and two non-ordinary SCBs on different surfaces are found. All the surface critical exponents obtained by various fits [41] to Eqs. (24), (25), and (26) are listed in Table II. For the reader's convenience, the surface critical exponents of other models are listed in Table III.

### A. Surface critical behaviors at $J_{c2}$

We first study the surface critical behaviors associated with the bulk critical point  $J_{c2}$  separating the Néel ordered phase from the RS phase.

We start by checking the SCB on the Y surface, referred to as ‘‘Y-c2.’’ The numerical result of  $\chi_{s1}$  as a function of size  $L$  is graphed in Fig. 8(a), and the results of  $C_{\parallel}(L/2)$  and  $C_{\perp}(L/2)$  as functions of  $L$  are plotted in Fig. 8(b).

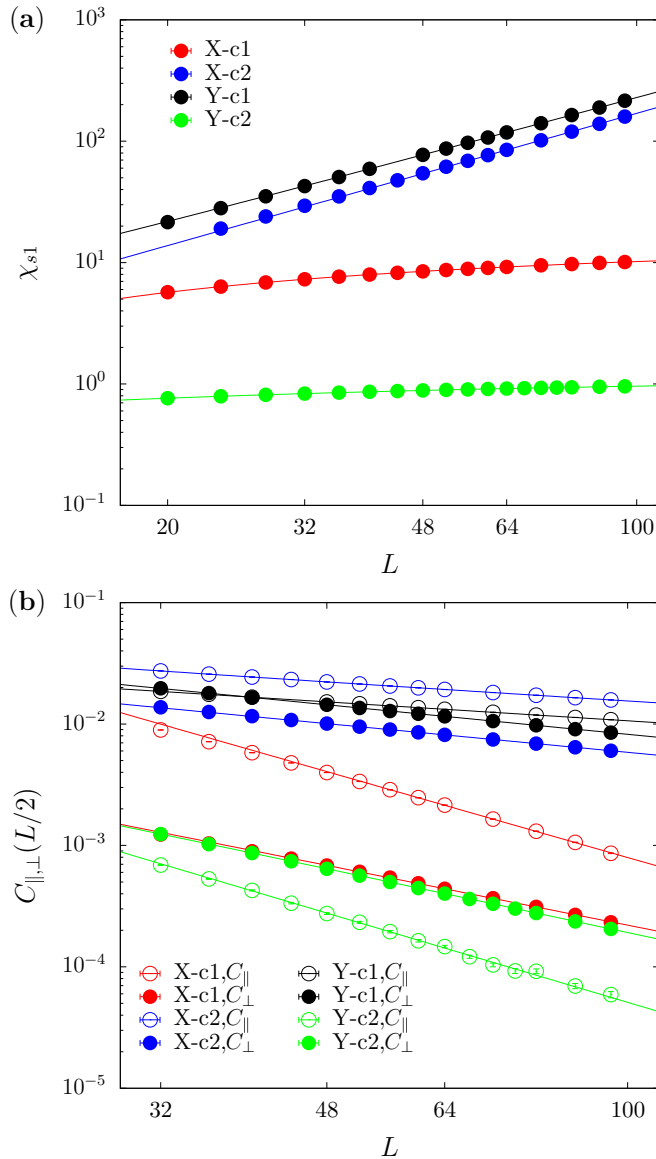


FIG. 8. Surface staggered magnetic susceptibility  $\chi_{s1}$  (a) and the correlations  $C_{||}(L/2)$  and  $C_{\perp}(L/2)$  (b) vs system size  $L$  for four surface configurations: X-c1, X-c2, Y-c1, and Y-c2. The plots are on log-log scale.

We fit the data of  $C_{||}(L/2)$  and  $C_{\perp}(L/2)$  according to Eqs. (24) and (25) and find statistically sound estimates of  $\eta_{||} = 1.318(31)$  and  $\eta_{\perp} = 0.682(6)$ .

The finite-size scaling form Eq. (26) supplemented with a constant  $c$  as nonsingular contribution, i.e.,

$$\chi_{s1} = c + aL^{-(2-2y_{h1})}(1 + bL^{-\omega}), \quad (29)$$

is used to fit the data of  $\chi_{s1}$ . The estimate of  $y_{h1}$  is 0.852(34), with  $\omega$  set to 1.

These surface exponents are listed in Table II. They obey the scaling relations in Eqs. (27) and (28), and agree well with the universal class of the ordinary transition associated with the 3D O(3) universality class found in various classical

and quantum phase transitions (see Table III). This behavior is expected since the surface state on the Y surface in the RS phase is gapped, as shown in Sec. III C.

We then check the SCBs at critical point  $J_{c2}$  on the X surface, referred to as “X-c2.” This is the case when the surface is made up of dangling spins.

The numerical result of  $\chi_{s1}$  as a function of size  $L$  is graphed in Fig. 8(a), and the results of  $C_{||}(L/2)$  and  $C_{\perp}(L/2)$  as functions of  $L$  are shown in Fig. 8(b). Data fitting according to Eqs. (24), (25), and (26) find statistically sound estimations  $\eta_{||} = -0.560(8)$ ,  $\eta_{\perp} = -0.259(4)$ , and  $y_{h1} = 1.780(2)$ , satisfying the scaling relations Eqs. (27) and (28).

The three exponents are also listed in Table II. They are consistent or very close to the nonordinary SCBs found in the quantum critical points of the 3D O(3) universality class [4,9,10,13]. This result supports the scenario that nonordinary SCB can be induced by the gapless surface mode on the dangling spin-1/2 surface, as explored in Sec. III C.

### B. Surface critical behaviors at $J_{c1}$

We then study the SCBs associated with the bulk critical point  $J_{c1}$  at which the SPT Haldane phase transfers to the O(3) symmetry broken Néel phase.

We first study the Y surface with associated SCB denoted by “Y-c1”. The surface does not consist of dangling spins. However, we have shown in Sec. III B that the state of the Y surface in the gapped SPT Haldane phase is gapless due to the spin-1/2 excitations located at the ends of each diagonal ladder.

The numerical results of  $C_{||}(L/2)$ ,  $C_{\perp}(L/2)$ , and  $\chi_{s1}(L)$  as functions of  $L$  are plotted in Fig. 8. Apparently, the SCBs on the Y surface (Y-c1) are similar to those of X-c2 at  $J_{c2}$ .

We fit the data of  $\chi_{s1}$ ,  $C_{||}(L/2)$ , and  $C_{\perp}(L/2)$  according to Eqs. (26), (24), and (25), respectively, and obtain statistically sound results  $y_{h1} = 1.756(3)$ ,  $\eta_{||} = -0.511(2)$  and  $\eta_{\perp} = -0.237(2)$ , as listed in Table II. These exponents satisfy the scaling relations Eqs. (27) and (28), and are consistent with or very close to the nonordinary SCB found on the X surface at  $J_{c2}$ , as well as those nonordinary SCBs found at other quantum critical points of the 3D O(3) universality class [4,9,10,13].

Finally, we check the SCBs on the X surface, referred to as “X-c1.” The surface is gapped in the Haldane phase, as shown in Sec. III B, as a result, the surface transition must belong to the ordinary class. Our numerical results verified that the SCBs are of the ordinary type.

The numerical results of  $C_{||}(L/2)$ ,  $C_{\perp}(L/2)$ , and  $\chi_{s1}(L)$  as functions of  $L$  are plotted in Fig. 8. The curves share similar slopes of the corresponding Y-c2 curves. Fitting these results according to Eqs. (24), (25), and (26), we obtain  $y_{h1} = 0.82(1)$ ,  $\eta_{||} = 1.36(5)$  and  $\eta_{\perp} = 0.69(2)$ , as listed in Table II. Again, they satisfy the scaling relations Eqs. (27) and (28), and agree well with the exponents of the ordinary class in the 3D O(3) universality class.

## V. DISCUSSION AND CONCLUSIONS

We have studied the spin-1/2 Heisenberg model on the 2D CDL lattice using quantum Monte Carlo simulations. We

showed that the model realizes a 2D SPT Haldane phase when the ladders are weakly coupled. By tuning the interladder coupling, the model enters the Néel ordered phase first, then the trivial product RS phase, through two quantum critical points. Furthermore, we demonstrated that the two QCPs are in the 3D O(3) universality class, whether the magnetically disordered phase is a topologically nontrivial SPT phase or the simple product RS phase.

We have also studied the properties of the two gapped phases, including the finite-size behaviors of two topologically distinct string order parameters in the Haldane phase. Compared with the previously studied models, this model has more abundant surface configurations. We showed that the Y surface, formed by the ends of the ladders, is gapless, while the X surface, exposed along the ladder, is gapful, in the Haldane phase. Conversely, in the gapped RS phase, the Y surface is gapped, and the X surface is gapless.

The mechanisms of the two gapless modes are different. One is due to the properties of a topological SPT state. The equivalent spin-1 chain of the diagonal ladder with free boundary conditions has a topological term of two spin-1/2 located at the boundaries. When the ladders are coupled to form a 2D system, the spin-1/2 excitations form a gapless edge state, according to the Lieb-Schultz-Mattis theorem. This explains the gapless Y surface in the Haldane phase. The other is due to the surface being formed by dangling spins. At least for spin-1/2 models, this can be understood by assuming that the dangling spins form a spin-1/2 Heisenberg chain, which is gapless due to the topological  $\theta$  term, suppressing the topological defects. This applies to the X surface in the RS phase.

We focused particular attention on the SCBs at the two bulk critical points. We have shown that the SCBs are always in the ordinary class on surfaces that are gapped in the gapped bulk phases. More importantly, we have demonstrated that nonordinary SCBs are realized at both critical points but only on the gapless surfaces of gapped bulk states exposed by

simply cutting bonds without fine-tuning the surface coupling, which is required to reach a multicritical point away from the ordinary class in the classical models.

Considering that the gapless surface states in the gapped bulk phase are intimately related to the nonordinary SCBs at quantum critical points, and the mechanisms that lead to such gapless surface states are quantum mechanical, our paper strongly supports the quantum origin of the nonordinary surface critical behaviors found in various quantum models.

Finally, we would like to point out that the nonordinary SCBs have been found in many quantum models, including various dimerized Heisenberg models, with spin-1/2 and spin-1, the 2D coupled spin-1 Haldane chains, and are now also found at two different critical points of the 2D coupled diagonal ladders on two different surfaces. The surfaces showing such nonordinary SCBs are exposed by simply cutting lattices without any tuning of surface couplings. It is hard to believe all these systems are, by chance, close to the special transition of the critical 3D classical O(3) model. Our findings call for further investigation.

#### ACKNOWLEDGMENTS

We thank Prof. H. Q. Lin and Dr. Wenjing Zhu for valuable discussions. This work was supported by the National Natural Science Foundation of China under Grants No. 12175015 and No. 11734002. The authors acknowledge support extended by the Super Computing Center of Beijing Normal University.

#### APPENDIX: A SUMMARY OF VARIOUS RESULTS

For the reader's convenience, the surface critical exponents of the coupled diagonal ladders (CDL), as well as other models at critical points in the 3D O(3) universality class are listed in Table III for comparison. Some field theoretical results from different methods are also listed for comparison.

TABLE III. For the reader convenience, the surface critical exponents of the coupled diagonal ladders (CDL), as well as other models at critical points in the 3D O(3) universality class are listed for comparison, with CHC the QCP of the coupled Haldane chains, CD-DAF the Dimer-AF QCP of the columnar dimerized Heisenberg model, SD-DAF the Dimer-AF QCP of the staggered dimerized Heisenberg models, DS-DAF and DS-PAF the Dimer-AF QCP and the PVBC-AF QCP of the dimerized Heisenberg model on the DS lattice, respectively, 3D CH the three-dimensional classical Heisenberg model. For the types of surface configurations, D denotes dangling and N nondangling. “class.” means classical model. For the SCB class, “Ord.” is the abbreviation of ordinary, “Nonord.” means nonordinary, and “Sp.” special. The field theoretical results (FT) from different methods are also listed for comparison.

SCB class	Model/methods	Surfaces	Spin S	$\eta_{\parallel}$	$\eta_{\perp}$	$\gamma_{h1}$
Nonord.	CDL	X-c2	1/2	-0.56(1)	-0.259(3)	1.780(2)
Nonord.		Y-c1	1/2	-0.511(2)	-0.237(2)	1.756(3)
Ord.		X-c1	1/2	1.36(6)	0.69(3)	0.82(1)
Ord.		Y-c2	1/2	1.318(31)	0.682(9)	0.852(46)
Nonord. [13]	CHC	x surface	1	-0.57(2)	-0.27(2)	1.760(3)
Ord. [13]		y surface	1	1.38(2)	0.69(2)	0.79(2)
Nonord. [9]	CD-DAF	D	1/2	-0.445(15)	-0.218(8)	1.7339(12)
Nonord. [10]		D	1/2	-0.50(6)	-0.27(1)	1.740(4)
Nonord. [12]		D	1	-0.539(6)	-0.25(1)	1.762(3)
Ord. [10]		N	1/2	1.30(2)	0.69(4)	0.84(1)
Ord. [9]		N	1/2	1.387(4)	0.67(6)	0.840(17)
Ord. [12]		N	1	1.32(2)	0.70(2)	0.80(1)
Ord. [9]	SD-DAF	N	1/2	1.340(21)	0.682(2)	0.830(11)
Nonord. [4]	DS-DAF	D	1/2	-0.449(5)	-0.2090(15)	1.7276(14)
Nonord. [10]		D	1/2	-0.50(1)	-0.228(5)	1.728(2)
Ord. [10]		N	1/2	1.29(6)	0.65(3)	0.832(8)
Ord. [4]	DS-PAF	N	1/2	1.327(25)	0.680(8)	0.810(20)
Ord. [10]		N	1/2	1.33(4)	0.65(2)	0.82(2)
Nonord. [10]		D	1/2	-0.517(4)	-0.252(5)	1.742(1)
Ord. [42]	3D CH		class.			0.813(2)
Ord. [43]	FT, 4-d $\epsilon$ -exp		class.	1.307	0.664	0.846
Ord. [44]	FT, d-2 $\epsilon$ -exp		class.	1.39(2)		
Ord. [45,46]	FT, Massive field		class.	1.338	0.685	0.831
Ord. [47]	FT, Conformal bootstrap		class.			0.831
Sp. [48]	FT, 4-d $\epsilon$ -exp		class.	-0.445	-0.212	1.723

- [1] J. Cardy, *Scaling and Renormalization in Statistical Physics*, Cambridge Lecture Notes in Physics (Cambridge University Press, Cambridge, 1996), Vol. 5, p. 238.
- [2] K. Binder, in *Phase Transitions and Critical Phenomena*, edited by C. Domb and J. L. Lebowitz, Vol. 8 (Academic Press, London, 1983), pp. 1–144.
- [3] H. W. Diehl, in *Phase Transitions and Critical Phenomena*, edited by C. Domb and J. L. Lebowitz, Vol. 10 (Academic Press, London, 1986), pp. 75–267.
- [4] L. Zhang and F. Wang, Unconventional Surface Critical Behavior Induced by a Quantum Phase Transition from the Two-Dimensional Affleck-Kennedy-Lieb-Tasaki Phase to a Néel-Ordered Phase, *Phys. Rev. Lett.* **118**, 087201 (2017).
- [5] N. D. Mermin and H. Wagner, Absence of Ferromagnetism or Antiferromagnetism in One- or Two-Dimensional Isotropic Heisenberg Models, *Phys. Rev. Lett.* **17**, 1133 (1966).
- [6] Z.-C. Gu and X.-G. Wen, Tensor-entanglement-filtering renormalization approach and symmetry-protected topological order, *Phys. Rev. B* **80**, 155131 (2009).
- [7] F. Pollmann, A. M. Turner, E. Berg, and M. Oshikawa, Entanglement spectrum of a topological phase in one dimension, *Phys. Rev. B* **81**, 064439 (2010).
- [8] X. Chen, Z.-C. Gu, Z.-X. Liu, and X.-G. Wen, Symmetry-protected topological orders in interacting bosonic systems, *Science* **338**, 1604 (2012).
- [9] C. Ding, L. Zhang, and W. Guo, Engineering Surface Critical Behavior of  $(2+1)$ -Dimensional O(3) Quantum Critical Points, *Phys. Rev. Lett.* **120**, 235701 (2018).
- [10] L. Weber, F. Parisen Toldin, and S. Wessel, Nonordinary edge criticality of two-dimensional quantum critical magnets, *Phys. Rev. B* **98**, 140403(R) (2018).
- [11] C. Ding, W. Zhu, W. Guo, and L. Zhang, Special transition and extraordinary phase on the surface of a two-dimensional quantum Heisenberg antiferromagnet, [arXiv:2110.04762](https://arxiv.org/abs/2110.04762).
- [12] L. Weber and S. Wessel, Nonordinary criticality at the edges of planar spin-1 Heisenberg antiferromagnets, *Phys. Rev. B* **100**, 054437 (2019).
- [13] W. Zhu, C. Ding, L. Zhang, and W. Guo, Surface critical behavior of coupled Haldane chains, *Phys. Rev. B* **103**, 024412 (2021).

- [14] F. D. M. Haldane, “ $\theta$  physics” and quantum spin chains (abstract), *J. Appl. Phys.* **57**, 3359 (1985).
- [15] A. Abanov, Topology, geometry and quantum interference in condensed matter physics, in *Texts and Readings in Physical Sciences*, edited by S. Bhattacharjee and A. Bandyopadhyay, Vol. 19 (Springer, Singapore, 2017).
- [16] K. Wierschem and P. Sengupta, Quenching the Haldane Gap in Spin-1 Heisenberg Antiferromagnets, *Phys. Rev. Lett.* **112**, 247203 (2014).
- [17] Y.-Z. You, Z. Bi, A. Rasmussen, K. Slagle, and C. Xu, Wave Function and Strange Correlator of Short-Range Entangled States, *Phys. Rev. Lett.* **112**, 247202 (2014).
- [18] E. Lieb, T. Schultz, and D. Mattis, Two soluble models of an antiferromagnetic chain, *Ann. Phys.* **16**, 407 (1961).
- [19] M. A. Metlitski, Boundary criticality of the  $O(N)$  model in  $d = 3$  critically revisited, *SciPost Phys.* **12**, 131 (2022).
- [20] C.-M. Jian, Y. Xu, X.-C. Wu, and C. Xu, Continuous Néel-VBS quantum phase transition in non-local one-dimensional systems with  $SO(3)$  symmetry, *SciPost Phys.* **10**, 033 (2021).
- [21] F. Parisen Toldin, Boundary Critical Behavior of the Three-Dimensional Heisenberg Universality Class, *Phys. Rev. Lett.* **126**, 135701 (2021).
- [22] F. Parisen Toldin and M. A. Metlitski, Boundary Criticality of the 3d  $O(n)$  Model: From Normal to Extraordinary, *Phys. Rev. Lett.* **128**, 215701 (2022).
- [23] J. Padayasi, A. Krishnan, M. A. Metlitski, I. A. Gruzberg, and M. Meineri, The extraordinary boundary transition in the 3d  $O(N)$  model via conformal bootstrap, *SciPost Phys.* **12**, 190 (2022).
- [24] E. H. Kim, G. Fáth, J. Sólyom, and D. J. Scalapino, Phase transitions between topologically distinct gapped phases in isotropic spin ladders, *Phys. Rev. B* **62**, 14965 (2000).
- [25] W. J. L. Buyers, R. M. Morra, R. L. Armstrong, M. J. Hogan, P. Gerlach, and K. Hirakawa, Experimental Evidence for the Haldane Gap in a Spin-1 Nearly Isotropic, Antiferromagnetic Chain, *Phys. Rev. Lett.* **56**, 371 (1986).
- [26] J.-P. Renard, L.-P. Regnault, and M. Verdaguer, Haldane quantum spin chains, in *Magnetism: Molecules to Materials* (John Wiley and Sons, Hoboken, NJ, 2004), Chap. 2, pp. 49–93.
- [27] E. Dagotto, Experiments on ladders reveal a complex interplay between a spin-gapped normal state and superconductivity, *Rep. Prog. Phys.* **62**, 1525 (1999).
- [28] A. W. Sandvik and J. Kurkijärvi, Quantum Monte Carlo simulation method for spin systems, *Phys. Rev. B* **43**, 5950 (1991).
- [29] A. W. Sandvik, Stochastic series expansion method with operator-loop update, *Phys. Rev. B* **59**, R14157 (1999).
- [30] K. Binder, Critical Properties from Monte Carlo Coarse Graining and Renormalization, *Phys. Rev. Lett.* **47**, 693 (1981).
- [31] K. Binder and D. P. Landau, Finite-size scaling at first-order phase transitions, *Phys. Rev. B* **30**, 1477 (1984).
- [32] E. L. Pollock and D. M. Ceperley, Path-integral computation of superfluid densities, *Phys. Rev. B* **36**, 8343 (1987).
- [33] A. W. Sandvik, Computational studies of quantum spin systems, *AIP Conf. Proc.* **1297**, 135 (2010).
- [34] M. P. A. Fisher, P. B. Weichman, G. Grinstein, and D. S. Fisher, Boson localization and the superfluid-insulator transition, *Phys. Rev. B* **40**, 546 (1989).
- [35] H. Shao, W. Guo, and A. W. Sandvik, Quantum criticality with two length scales, *Science* **352**, 213 (2016).
- [36] R. Guida and J. Zinn-Justin, Critical exponents of the  $N$ -vector model, *J. Phys. A: Math. Gen.* **31**, 8103 (1998).
- [37] M. Hasenbusch and E. Vicari, Anisotropic perturbations in three-dimensional  $O(n)$ -symmetric vector models, *Phys. Rev. B* **84**, 125136 (2011).
- [38] I. Affleck, T. Kennedy, E. H. Lieb, and H. Tasaki, Rigorous Results on Valence-Bond Ground States in Antiferromagnets, *Phys. Rev. Lett.* **59**, 799 (1987).
- [39] M. den Nijs and K. Rommelse, Preroughening transitions in crystal surfaces and valence-bond phases in quantum spin chains, *Phys. Rev. B* **40**, 4709 (1989).
- [40] F. Anfuso and A. Rosch, Fragility of string orders, *Phys. Rev. B* **76**, 085124 (2007).
- [41] P. Young, Everything you wanted to know about data analysis and fitting but were afraid to ask, *SpringerBriefs in Physics* (Springer, New York, 2015).
- [42] Y. Deng, H. W. J. Blöte, and M. P. Nightingale, Surface and bulk transitions in three-dimensional  $O(n)$  models, *Phys. Rev. E* **72**, 016128 (2005).
- [43] H. Diehl and S. Dietrich, Scaling laws and surface exponents from renormalization group equations, *Phys. Lett. A* **80**, 408 (1980).
- [44] H. W. Diehl and A. Nüsser, Critical Behavior of the Nonlinear  $\sigma$  Model with a Free Surface: The “Ordinary” Transition in  $2+\epsilon$  Dimensions, *Phys. Rev. Lett.* **56**, 2834 (1986).
- [45] H. W. Diehl and M. Shpot, Surface Critical Behavior in Fixed Dimensions  $d < 4$ : Nonanalyticity of Critical Surface Enhancement and Massive Field Theory Approach, *Phys. Rev. Lett.* **73**, 3431 (1994).
- [46] H. Diehl and M. Shpot, Massive field-theory approach to surface critical behavior in three-dimensional systems, *Nucl. Phys. B* **528**, 595 (1998).
- [47] F. Gliozzi, P. Liendo, M. Meineri, and A. Rago, Boundary and interface CFTs from the conformal bootstrap, *J. High Energy Phys.* **05** (2015) 036.
- [48] H. W. Diehl and S. Dietrich, Field-theoretical approach to multicritical behavior near free surfaces, *Phys. Rev. B* **24**, 2878 (1981).